Chemical Engineering Journal 158 (2010) 2–10

Contents lists available at ScienceDirect

Chemical Engineering Journal

journal homepage: www.elsevier.com/locate/cej

High-speed chemical species tomography in a multi-cylinder automotive engine

Paul Wright[a,*], Nataša Terzija[a], John L. Davidson[a], Sergio Garcia-Castillo[a], Charles Garcia-Stewart[a], Stephen Pegrum[b], Steve Colbourne[b], Paul Turner[b], Sam D. Crossley[c], Tim Litt[c], Stuart Murray[c], Krikor B. Ozanyan[a], Hugh McCann[a]

[a] School of Electrical & Electronic Engineering, University of Manchester, Sackville St., Manchester M60 1QD, UK
[b] Roush Technologies Ltd., Brentwood, UK
[c] AOS Technology Ltd., Melton Mowbray, UK

ARTICLE INFO

Article history:
Received 6 May 2008
Received in revised form 15 October 2008
Accepted 17 October 2008

Keywords:
Tomography
NIR
Optical
Combustion engine

ABSTRACT

We report here the first application of chemical species tomography (CST) in a multi-cylinder automotive engine. This technique offers high-speed continuous imaging of hydrocarbon fuel distribution and mixing within the combustion chamber and is therefore of interest to both engine designers and combustion scientists. Many of the methods described are equally applicable to chemically selective imaging of other highly dynamic mixing and reaction processes.

A measurement grid consisting of 27 dual-wavelength optical paths has been implemented in one cylinder of an otherwise standard four-cylinder port-injected gasoline engine, using a unique OPtical Access Layer (OPAL) carrying embedded optical fibres and collimators. The OPAL provided adequate performance on many beams for more than 2 h of fired engine operation. To improve sensitivity and to cope with fuel spray injection directly into the cylinder (in other engine types), a low-noise opto-electronic system has been developed, offering laser intensity modulation at frequencies up to 1 MHz. Dual-wavelength measurements are recorded on each channel at 100 kSPS, prior to off-line processing that typically reduces the effective frame rate to 3000–4000 frames/s, dependent upon engine speed. The performance of the system is assessed, using running conditions chosen to provide a qualitatively known (homogeneous) fuel distribution for validation purposes. Examples of measured data and processing schemes are discussed. Sample tomographic images, obtained using a novel quality-based approach to data selection, are presented.

1. Introduction

The spatial distributions of reactants are first-order determinants of the behaviour and performance of many types of chemical reactor. In the face of demanding environmental legislation [1], product viability in the automotive industry is crucially dependent on the chemical reaction performance of the internal combustion engine. Driven by this imperative, automotive engineering researchers in both academia and industry have developed a range of in situ techniques for imaging gaseous fuel distributions within engines, particularly within the combustion chamber [2]. In this paper, we report the application of the relatively new technique of dual-wavelength Near-InfraRed Absorption Tomography (NIRAT) [3,4] to high-speed in-cylinder imaging of standard unleaded gasoline fuel in a multi-cylinder engine.

The ideal system for imaging in-cylinder gaseous fuel distribution would be:

(1) non-intrusive to in-cylinder flow and combustion processes;
(2) directly sensitive to the fuel, without the use of artificial dopants;
(3) capable of imaging real multi-component road fuels, as well as reference fuels, such as iso-octane;
(4) sensitive over a wide dynamic range of fuel concentration, from hundreds of parts per million by volume (ppm) to tens of thousands of ppm;
(5) capable of spatially resolving all in-cylinder flow scales, i.e. from about 2 mm up to large fractions of the cylinder diameter (D);
(6) capable of providing continuous sub-cycle images with temporal resolution equivalent to intervals between images of only a few degrees of crank shaft rotation (°CA);

* Corresponding author. Tel.: +44 161 3064785; fax: +44 161 3064789.
E-mail addresses: paul.wright@manchester.ac.uk (P. Wright), H.McCann@manchester.ac.uk (H. McCann).

1385-8947/$ – see front matter © 2008 Elsevier B.V. All rights reserved.
doi:10.1016/j.cej.2008.10.026

(7) robust against non-species-specific optical effects;
(8) robust against the hostile thermodynamic environment of the engine;
(9) applicable to multi-cylinder road-going engines with minimal modification, as well as specialized single-cylinder research engines;
(10) free of potential additional hazards beyond those inherent in the engine test cell environment.

No technique has yet been demonstrated that satisfies all of the preceding requirements but several, predominantly of an optical nature, have been developed that offer partial solutions [2,5]. By far the most successful in-cylinder fuel imaging technique to date is Planar Laser-Induced Fluorescence (PLIF), which has been widely used for studies of fuel-air mixture preparation and combustion processes for over 20 years. It continues to be extensively developed [6] due to its inherently excellent spatial and temporal resolution. Nevertheless, quantitative PLIF imaging of hydrocarbon fuels requires the use of fluorescent dopants and hence cannot be applied directly to commercial fuels [7] and its inherent requirement for multi-planar optical access makes it overwhelmingly difficult to apply to multi-cylinder engines. NIRAT can address these shortcomings, albeit at the expense of greatly reduced spatial resolution. Significantly, its modest optical access requirements and direct sensitivity to hydrocarbon fuels allow its use at all stages of the development process, from initial flow bench studies, through single-cylinder engine tests, to final design validation of multi-cylinder implementations.

The concept of chemically selective optical tomography has long been discussed in the literature, but has only recently been implemented in practical form for *dynamic* processes. Philipp et al. [8] describe 'passive' systems that exploit the optical emission from the in-cylinder flame to provide a limited insight into the preceding fuel distribution. Other non-chemically selective forms of optical tomography have been reported, which afford high temporal resolution by enabling simultaneous acquisition of distributed measurements through the subject, e.g. Snyder and Hesselink [9] used a holographic interferometry technique that exploits variations in the index of refraction in the subject, although this requires very large-scale optical access. We will not discuss either of these two classes of systems further, since we are concerned here only with situations where a light source with properties chosen and controlled by the user is directed through the process in order to achieve chemical selectivity and permit time-resolved imaging.

Early studies of this type by Santoro et al. [10] used a laser source and a detector, to form a single-beam absorption measurement system, which was translated across/rotated around the subject. The light source employed was a He–Ne laser, emitting 3.39 μm light that was used to image methane in jets of pre-mixed air (90%) and methane (10%). This general approach served as the basis for many studies in the 1980s and 90s: experimental activities were restricted to subjects with slow spatial variation, and many authors carried out simulation and image reconstruction of the data thus obtained [11,12]. Although this implementation of the tomographic technique achieves the desired chemical selectivity, it is clearly not appropriate for non-steady subjects.

Using broad-band sources, Barrag and Lawton [13], Shimizu and Sakai [14] and Krämer et al. [15] achieved high-speed optical tomography by simultaneous application of multiple beams to the subject. Wavelength selection (to achieve specificity) was performed after transmission through the subject, by the use of either interchangeable filters or dispersive detection. In all cases, the selected optical configurations placed severe restrictions on the applications of these techniques, although Barrag and Lawton attempted to ameliorate this problem by using optical fibres in both the light launch and receive sub-systems, at the cost of obtaining absorption measurements along only 8 beam paths. Both Barrag and Lawton (soot distribution), and Krämer et al. (hydrocarbon distributions) presented the application of their techniques to single-cylinder engines. Another notable development during the 1990s was the improvement of optical absorption measurement techniques to cope with attenuation due to non-species-specific effects, e.g. by Drallmeier [16], who simultaneously used two wavelengths (from a visible laser emitter and the mid-IR He–Ne) to take account of scattering.

The emergence of diode lasers, high-specification fibre systems and detectors for the Near-IR made it possible to develop CST systems with a degree of robustness appropriate to the needs of process applications, with the elimination of open-path optics being a significant step forward in this respect. The innate high-frequency capabilities of diode laser sources and photodiode detectors permit very fast and continuous imaging, and the use of different and/or multiple sources affords access to a range of different chemical species as well as providing reference measurements. This so-called All-Opto-Electronic form of CST was first developed and demonstrated in the Manchester NIRAT system [3,4,17], using 4 projections, each comprising 8 parallel beams, to yield 32 simultaneous beam path measurements and achieving 3500 frames/s for hydrocarbons in an engine simulator. Salem et al. [18], seeking to measure water distribution above a fixed-bed adsorber column, demonstrated an alternative laboratory implementation of CST using a single diode laser source operated in wavelength scanning mode. Three projections were generated using open-path light sheets which, when viewed by array detectors, yielded 384 simultaneous beam path measurements.

We have discussed previously [17] the practicality of applying the Manchester NIRAT technique to multi-cylinder spark-injected (SI) engines. Here, we present validation tests of the completed system as implemented on a 4-cylinder gasoline engine, running under conditions intended to produce a homogeneous fuel distribution. Examples of the data obtained and the resulting tomographic images are presented. A related publication [19] describes preceding laboratory tests using the system, with particular emphasis on image reconstruction techniques and the validation of imaging performance on laboratory phantoms, including both homogeneous and inhomogeneous subjects.

2. System implementation

The tomography system discussed here was developed for the IMAGER project and is a 32-channel hard-field instrument, optimised for in-cylinder application. A schematic representation of the system is given in Fig. 1. It comprises an OPtical Access Layer (OPAL), which defines the measurement beam layout within the engine, and a rack-mounted opto-electronic measurement system. The engine and OPAL combination was mounted on a dynamometer and connected, via fibre optic links, to the measurement system, located outside of the test cell.

2.1. Measurement system

To measure the path concentration integral (PCI) of the target species, the system implements a dual wavelength ratiometric (DWR) transmission measurement, as discussed in [17]. For convenience, we restate here the expression for the PCI of a spatially varying target-species concentration c, along a path of length L, in terms of the incident and received light intensities, $I_0(\lambda)$ and $I_r(\lambda)$

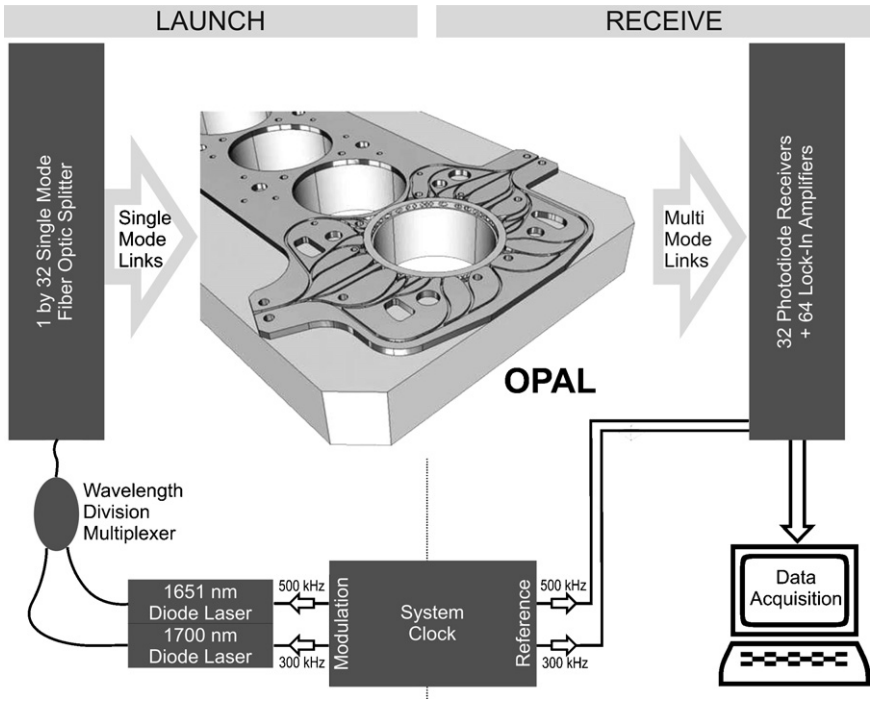

Fig. 1. Schematic overview of the IMAGER system; the OPAL is shown mounted on its transport plinth.

respectively, at two different wavelengths λ:

$$\int_L c.dl = \frac{1}{k(\lambda_1) - k(\lambda_2)} \ln\left(\frac{I_r(\lambda_2)}{I_r(\lambda_1)} \cdot \frac{I_0(\lambda_1)}{I_0(\lambda_2)}\right) \quad (1)$$

where $k(\lambda)$ is the wavelength-dependent absorption coefficient of the species in the gas mixture, λ_1 is selected to give measurable absorption by the target species, and λ_2 is a nearby reference wavelength chosen for its low absorption by the target species and by any other species in the gaseous mixture. The measurement system employs two fibre-coupled laser sources, a 1700 nm device for hydrocarbon (HC) sensing and a 1651 nm unit as a non-specifically absorbed reference. Custom laser drive electronics (AOS Technology Ltd., UK) provide temperature and current control. Each source has a maximum output (in fibre) of 3 mW and can be directly modulated at up to 1 MHz. A 4-channel direct digital synthesis (DDS) module provides modulation signals, at nominally 300 kHz and 500 kHz, to the laser drivers and phase shifted versions of these same frequencies to the lock-in amplifiers used for signal recovery. The DDS sub-system achieves high spectral purity (55 dBc SFDR), necessary to suppress the detection of optical signals at harmonics of the modulation frequencies, and allows software control of the frequency, amplitude and phase of the modulation/reference signals. The selected combination of modulation frequencies and optical wavelengths is intended to maximise the efficacy of the DWR approach, as described in [17]. An integrated wavelength division multiplexing (WDM) fibre coupler and 1×32 splitter (Sifam Fibre Optics, UK) connects the sources to the launch channels of the OPAL, via single mode fibre links. All fibre joints within the system either employ angled physical contact (APC) connectors or are fusion spliced, to aid in the suppression of optical noise. The design of the OPAL itself is discussed in the following section. Multimode fibres couple the collected light from each receive channel of the OPAL to a bank of 32 receivers, based on extended InGaAs photodiodes (G8421, Hamamatsu Photonics). The receiver design employed adds little excess noise (typically 3 dB) to the shot noise of a full scale transmission signal, although its relative contribution will inevitably increase as fouling of the OPAL reduces the collected signal power [20]. Each receiver feeds a pair of hybrid lock-ins, which recover and sample the demodulated transmission signal at each wavelength. The hybrid architecture offers adequate performance for this measurement and was preferred to a directly sampled approach on grounds of cost and power consumption. 12-bit sampling is used to avoid unnecessary degradation of the signal to noise ratio (SNR) of the transmission measurements. Centralised control of analogue to digital converter timing allows essentially simultaneous capture of all 64 measurements within each frame. A high-speed digital data controller, based on a programmable logic device, manages the transfer of data from each lock-in to a PC, via a digital data acquisition card (PCI-6534, National Instruments), as well as providing an interface for a rotary encoder, connected to the engine crankshaft. Acquisition and data transfer take place at a constant 10^5 frames per second. The system hardware and data structures allow alternative modules to replace unused optical channels, e.g. to provide synchronous capture of data from an in-cylinder pressure transducer, subject to a limit of 64 12-bit measurements overall.

The use of a high sampling rate has significant advantages in this application: (1) transient phenomena can be accurately measured as the system is not reliant upon averaging or accumulation of data across cycles; (2) the significant degree of oversampling allows post-processing to trade a reduction in effective sample rate for increased precision; (3) the hardware anti-alias filter, preceding the ADC, can have its cutoff located well above the (software) filtering used to set the lock-in detection bandwidth, ensuring accurately matched filtering of the data to be ratioed. These software filters are typically 8th order Bessel responses of 17.5 kHz cutoff frequency. The transmission value at each wavelength is then calculated by taking the mean of all samples within some specified crank angle interval. This interval is usually chosen to be 3°CA, yielding $2R$ frames per second, where R is the engine rotation rate in rpm. Both the software filtering and averaging are performed offline, allowing the same engine data to be analysed in several ways, e.g. at different levels of angular resolution.

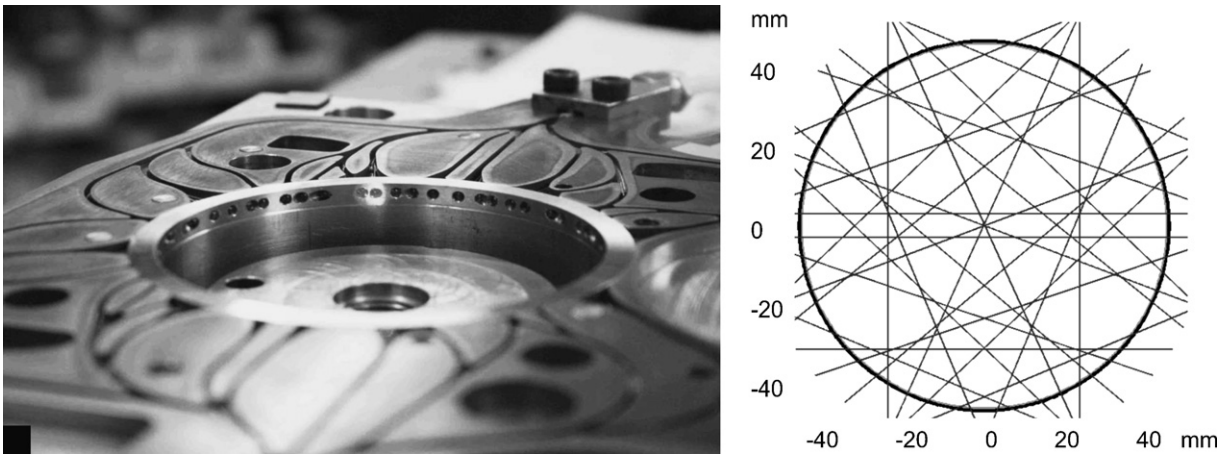

Fig. 2. (a) The OPAL during manufacture: fibre protection channels, coolant galleries and a fibre entry/exit port (upper right) are all clearly visible. (b) The 27 beam arrangement implemented by the present OPAL.

2.2. OPAL

Collection of transmission data requires accurate and highly stable positioning of the launch and receive optics within the combustion chamber; acceptable beam alignment must be maintained during rapid variations of both pressure (0–30 bar) and temperature (−30 to more than +150 Celsius). This led the authors to adopt a relatively thick (≈5 mm) and rigid OPAL structure (Fig. 2(a)), very different from the 'optical gaskets' that have been used in emission-based studies (e.g. [8]). This structural independence allows the beam grid to be developed, and indeed operated, wholly outside of the engine, as described in [19]. The launch and acceptance angles are controlled by collimation optics embedded within the structure of the OPAL. This helps to ensure that the hard-field assumption (whereby each measurement is influenced only by material that lies along its geometrical beam path) remains valid, even in the presence of moderate scattering. If the geometrical beam arrangement implemented by the OPAL is to be successful, its design must consider not only the opto-mechanical engineering problem but also the ultimate objective of tomographic image reconstruction. This requirement is readily understood from a signal processing perspective as the beam layout adopted defines the sampling of the Radon transform space. These issues are discussed in [19]. The resulting 27-beam arrangement (Fig. 2(b)) is highly optimised for the present engine. The OPAL replaces the uppermost portion of the engine block, so as to maintain the correct compression ratio, and includes all of the various oil and coolant galleries present in the standard engine. The optical fibres are located in protection channels within the OPAL, exiting via two ports on its perimeter into protective sleeves. This arrangement has proved robust; the current OPAL has endured several hours of both fired and motored (engine rotated under dynamometer control, without combustion) operation, at loads and speeds from unloaded idling up to 8 bar brake mean effective pressure (BMEP) at 4000 rpm. Within this range, the sealing integrity and thermal performance of the engine are not noticeably impaired, in keeping with our general aim of minimal modification of engine form and function. Inevitably, progressive fouling of the lenses leads to attenuation of the optical signals. The time taken for this to become significant depends markedly on the running conditions but up to 1 h of fired operation has been possible before lens cleaning becomes essential. The OPAL has been cleaned several times but the degradation of the optical signal levels has been found to be only partially reversible. Again, the extent of this depends on the running conditions but 3-6 dB of residual (post-cleaning) loss is typical following an hour of fired operation.

3. Data collection and analysis

An extensive program of both fired and motored testing has been undertaken, covering many load and speed combinations, but here we focus on running conditions chosen to yield an approximately known fuel distribution for validation purposes. Opportunities to achieve such a condition in a production engine are very limited but constitute an important step in extending what has been accomplished in laboratory phantoms [19] to the in-cylinder context. The homogeneous case is uniquely well suited to this calibration/validation task; the homogeneity of the resulting images can be quantified, the actual fuel concentration can to some extent be estimated from the incoming mass flow rate, and direct comparisons with results from the homogeneous laboratory phantom described in [19] are possible. All tests were carried out on an advanced dynamometer facility that allowed both steady-state and transient studies to be performed. Complementary measurements, including cylinder pressure and exhaust gas analysis, were made concurrently. All tests were performed on a 4-cylinder, in-line Ford Duratec (New I4) engine with 2.0 L capacity (89 mm bore), naturally aspirated, using port fuel injection. For the experiments reported here, the engine was first run in steady state, with the coolant temperature at typically 90 °C. The liquid fuel was injected onto the back surfaces of the inlet valves during the exhaust stroke, to promote rapid vaporisation. Inlet valve opening occurs at 5 °CA before top-dead-centre (TDC) of the exhaust stroke (i.e. virtually at the start of the induction stroke) and they remain open for 230 °CA (i.e. significantly into the compression stroke). Under these conditions, it is expected that, during the remainder of the compression stroke, the fuel will be efficiently vaporised and distributed relatively homogeneously, thereby yielding a suitable subject for validation tests. It should be noted that the engine selected is a current production unit, which achieves stage IV emissions standards and has been extensively developed for minimum engine-out HC emissions whilst operating at an assumed homogeneous state in-cylinder at stoichiometry. The example data presented here were collected with the engine running at 1500 rpm and 1.5 bar BMEP load. All tests were carried out using a standard commercial unleaded gasoline, with no added dopants.

In common with other in-cylinder measurement techniques, the raw data require considerable pre-processing prior to interpretation. Following time-domain filtering, ratiometric transmission

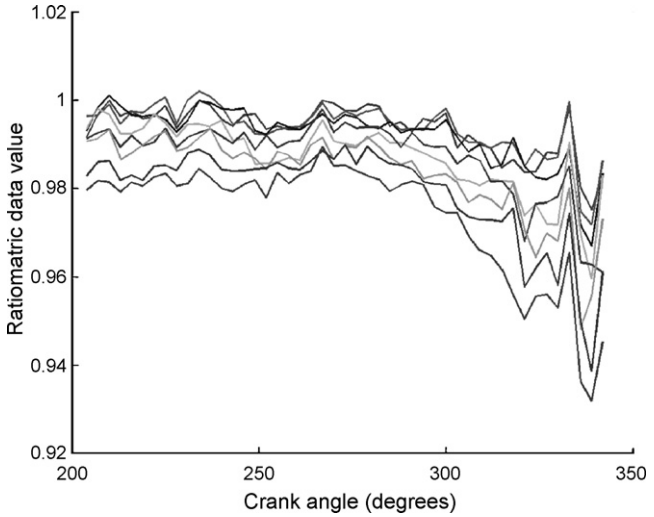

Fig. 3. Example of data after filtering, transformation to crank angle form and referencing against a motored cycle. The data shown are taken from 8 successive cycles of fired operation. TDC corresponds to 360 °CA in these plots.

values (T_{1700}/T_{1651}) are calculated. These are then re-expressed as a function of crank angle and averaged over typically 3 °CA blocks. Next, a referencing procedure is applied in which comparison of fired and motored cycles is used to suppress artefacts in the data that are unrelated to the HC distribution, for instance those arising from pressure-induced deformation of the engine block. Fig. 3 shows ratiometric transmission data, collected from eight successive cycles of fired operation that have been processed in this manner. Good repeatability is observed across all cycles. All eight show a general decrease in the ratio value as TDC is approached, corresponding to the increase in the volumetric concentration of HC as compression takes place. The magnitude of this change is broadly what would be expected from the measured fuel consumption at this engine speed and load, assuming an absorption coefficient in the range 100–165 $L\,mol^{-1}\,m^{-1}$. Several features are evident that may have been incorrectly categorised as measurement noise were they not present in successive cycles, most obviously the strong peak in the vicinity of 330°CA, underlining the value of continuous imaging in this application. Significant cycle-to-cycle variation remains, despite the applied referencing. The use of an intra-cycle reference, e.g. scaling each cycle to achieve a ratio value of unity at some arbitrary crank angle, has been investigated as a means to reduce this variability but has proved difficult to apply in practice and lacks the robust physical justification of our present method. Instead, recent efforts have focused on selection of the most appropriate motored reference data for a given dataset, to ensure suppression of uncontrolled factors is maximised. A 'skip-motored' strategy, in which short periods of fuel-free motoring are interleaved into the data collection process, has been used to provide reference conditions in close temporal proximity to the fired cycles being imaged. In keeping with our wish to achieve high temporal resolution, very little filtering has been applied to these data. The 3 °CA averaging process is the dominant response and has window length 0.33 ms at this engine speed. The typical SNR of individual beam path data is therefore modest; around 40 dB early in the OPAL's service life but falling over time as the fouling of the lenses increases. This is much inferior to the laboratory performance of the instrument (with an unused OPAL), where SNR's on some channels exceed 55 dB, highlighting the difficulties of in-cylinder studies. However, as will be seen below, the spatial filtering introduced during the reconstruction process is sufficient to yield useful imaging of the HC distribution from data of this quality.

Prior to image reconstruction, a qualification test was applied to the ratiometric transmission data from each beam. Specifically, we rejected beams that either retained more than 5% peak to peak noise in the ratiometric transmission data after 3 °CA averaging or that exhibited physically implausible behaviour, viz. ratiometric transmission showing values above 1.005 or a significantly increasing trend over the compression stroke as a whole. This prevents the resulting image being impaired by the inclusion of poor quality data, e.g. those with unacceptably low SNR due to heavily contaminated lenses. Therefore, in the images presented in this paper, various subsets of the 27 available beams are used for reconstruction, so as to always use the best available combination of data. The authors are unaware of previous use of this kind of dynamic selection concept in a tomographic system. In cases with an otherwise regular sampling of the Radon transform space, such an approach does limit the choice of reconstruction strategy to those methods able to handle incomplete data. Here, however, we are already dealing with an irregular distribution of measurements so the only penalty associated with data selection of this kind is an increase in the sparsity of sampling.

The tomographic images presented in Fig. 4 are obtained from the preceding ratiometric data using the iterative median filtered Landweber method described in [19]. Throughout this paper, we present relative HC concentration distributions across the imaging plane, which are also consistently scaled across crank angle. However, the difficulties of creating accurately known conditions within the combustion chamber mean that we do not as yet consider the technique proven to be fully quantitative within the engine context. For calculation purposes, we assume that pressure and temperature are constant across the measurement plane within a given frame. The C–H combination/overtone band used in this work exhibits far lower variation of absorption coefficient with pressure ($|\partial k/\partial P| \leq 11\ L\,mol^{-1}\,m^{-1}\,bar^{-1}$) than would typically be expected from a fundamental absorption line. This, along with the minimal change of absorption coefficient with temperature, reduces the significance of any departure from the above assumption. Within the forward model, the absorption coefficient is taken as being independent of temperature. The pressure value for a given frame is calculated from the crank angle by reference to a lookup table derived from 500-cycle averages of data from an in-cylinder pressure sensor. A second lookup process then yields the appropriate absorption coefficient at that pressure from a model fitted to the data shown in Fig. 1 of [17]. This approach is appropriate for the essentially steady-state running conditions described here but we anticipate a need for simultaneous collection of transmission and pressure data when studying some transient phenomena. To facilitate comparison, all of the images presented in this paper use consistent reconstruction parameters (50×50 image space, 7×7 median filter, 0.01 relaxation parameter, 50 iterations), which have been found to perform well for all available datasets, and use the global scale shown in Fig. 5(e). Outside of a validation context, computationally efficient initial conditions, e.g. the previous solution (or a homogeneous distribution based on the mean thereof), are likely to be preferred but here an initial zero HC distribution is assumed in all cases, to preserve the temporal independence of successive frames. Each row of Fig. 4 represents one of six consecutive fired cycles. The images shown cover the period of the compression stroke between 150 °CA and 30 °CA before TDC at intervals of 30° of crank angle. All images in Fig. 4 are obtained using data from a 15-beam subset of the full measurement grid (Fig. 5(a)). The 15 beams selected were those meeting the data quality requirements throughout all six cycles. Each cycle shows a similar development of spatial fuel distribution with crank angle, despite the previously mentioned variability in the underlying single-beam data. The aggregation of information and spatial filtering that take place

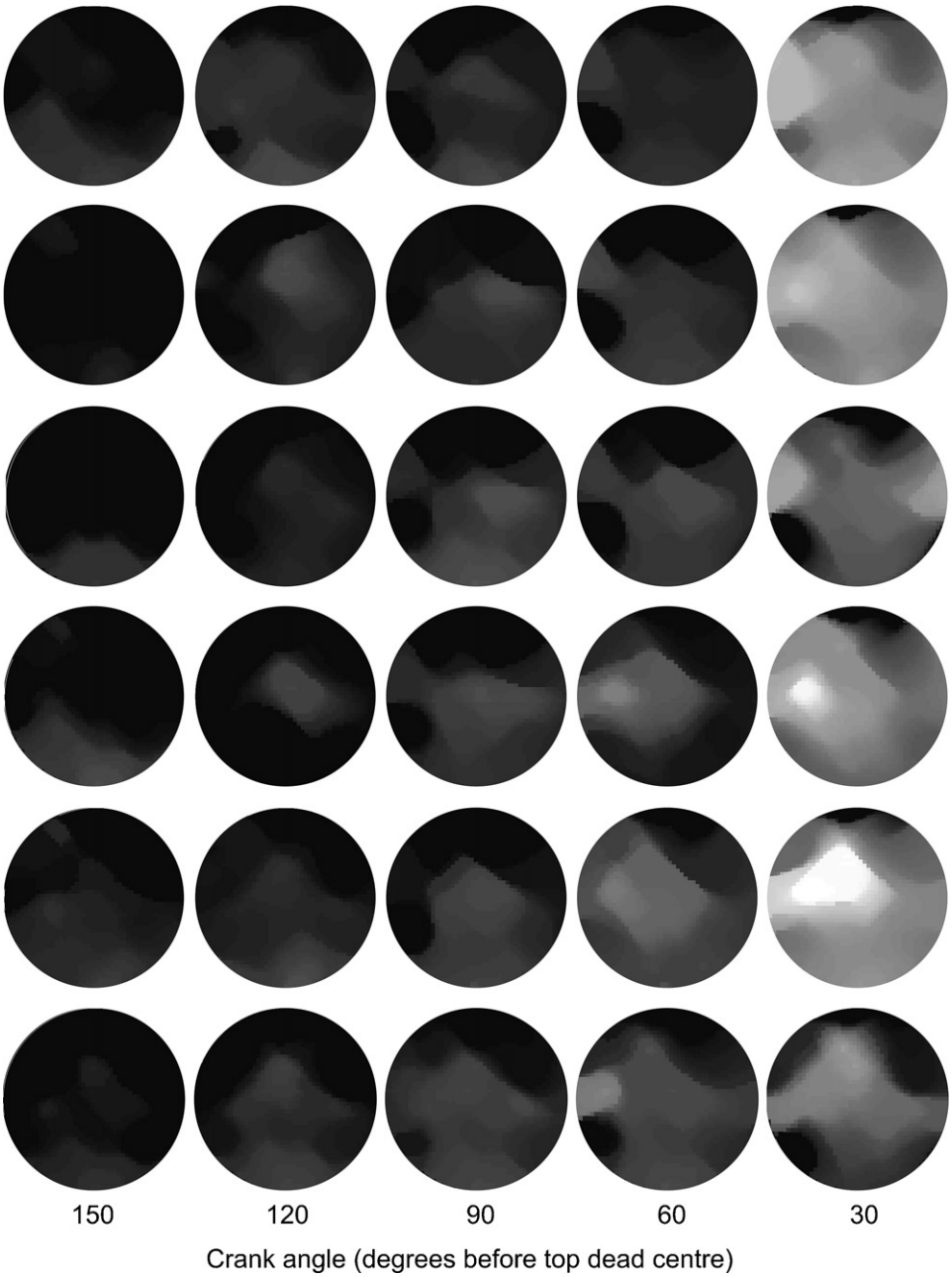

Fig. 4. Sequence of images reconstructed from data collected on an engine running at 1500 rpm and 1.5 bar BMEP load. Under these conditions the fuel distribution is expected to be homogeneous. Each row represents one of six successive fired cycles, over the period between 150 °CA and 30 °CA before TDC, at intervals of 30° of crank angle. An identical 15-beam subset of the OPAL's measurement paths, consisting of only those beams meeting the quality criteria across all six cycles, is used throughout, to maximise comparability both within and between cycles.

within the reconstruction process results in a remarkably consistent interpretation of the measurement data. It is apparent that the reconstructed estimate of the HC distribution is quite homogeneous, as is expected under these running conditions, and that the HC absorption increases sharply as the piston approaches TDC, corresponding to the rise in the volumetric concentration of the HC vapour. The authors believe that the apparently low HC concentration in the uppermost portion of each image is an artefact caused by the lack of measurement data in this region. This part of the engine block offers limited scope for the mounting of collimators, due to the proximity of the adjacent cylinder and, in Fig. 4, this problem was exacerbated by the loss of some beams due to lens fouling. Reconstructions of data derived from *simulated* homogeneous HC distributions exhibit similar features when the same 15-beam subset is used (Fig. 5(b)). For comparison, Fig. 5 also shows reconstructions of the same simulated homogeneous distribution using the 21-beam subset referred to in Fig. 6 and for the full 27-beam case. These three reconstructions use an absorption coefficient value of 107 L mol^{-1} m^{-1}, to allow comparison with experimental data 30° before TDC. Even when using such accurate and noiseless simulated data, the 27-beam arrangement only achieves modest spatial uniformity (±11% peak to peak, S.D. = 7%), placing an upper bound on the attainable imaging performance and emphasising the underdetermined nature of the problem. A significant increase in the number of beams is unlikely with current technologies (the 27-beam arrangement allows only 5.2 mm

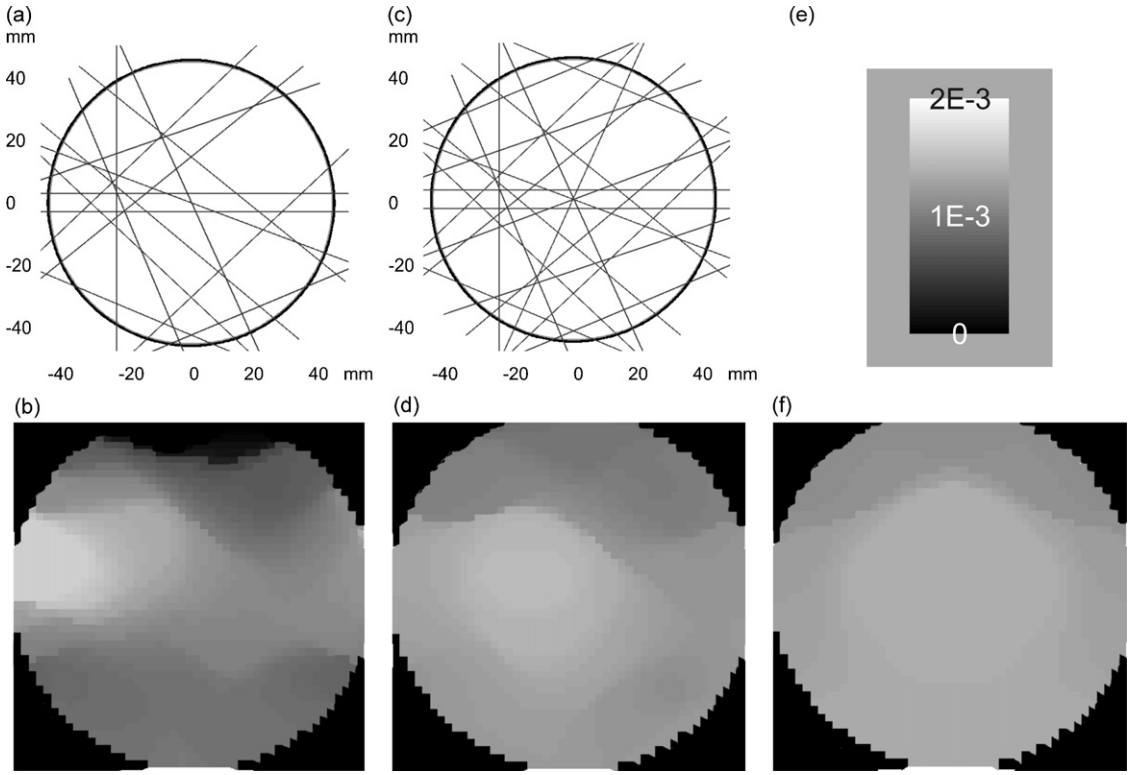

Fig. 5. Artefact generation during reconstruction of simulated homogeneous distributions due to limited beam coverage: (a) 15-beam subset used in Figs. 4 and 7; (b) image reconstructed from 15-beam subset; (c) 21-beam subset used in Fig. 6; (d) image reconstructed from 21-beam subset; (e) global colour scale used for all images in this paper (arbitrary units); (f) image reconstructed from full 27-beam data. All images use an absorption coefficient of 107 L mol^{-1} m^{-1} to allow comparison with the 30 °CA before TDC experimental images.

of cylinder wall per collimator on average, inclusive of the space needed for alignment) so this underdetermined situation should, at present, be considered as characteristic of the application. Despite evident differences between the three images considered in Fig. 5, the mean pixel value in each case is relatively stable, falling by around 1.5% in moving from 27 to 21 beams and by around 11% for the 27- to 15-beam case. Qualitatively, the existence of similar features in reconstructions of experimental and simulated data for each given beam subset supports the view that many are artefactual in nature. Strong similarities are also evident in the statistical properties of corresponding experimental and simulated data images (the standard deviation of the final image in the first row of Fig. 4 is almost identical to that of Fig. 5(b)) but a marked reduction in spread is associated with increasing the number of beams. The normalised root-mean-square difference between 15-beam reconstructions of experimental and simulated data is typically 18%, falling to around 12% in the 21-beam case. Image reconstruction apart, it should be recognised that the system delivers up to 27 individual in-cylinder path transmission measurements that can be used directly, e.g. in the validation of CFD modeling results.

The loss of any *valid* data is clearly undesirable, as evidenced by Fig. 5. The approach used for the generation of Fig. 4, in which a beam is disqualified globally for breaching the validity criteria within any cycle, allows the most direct inter-cycle comparison to be made. It is, however, rather wasteful of data; a slightly different approach to dynamic data selection is sometimes advantageous. The engine cycle depicted in the first row of Fig. 4 was actually found to have 21 beams satisfying the criteria when considered in isolation. Inclusion of the data from the six beams previously rejected yields a reconstructed fuel distribution much closer to the expected homogeneous behaviour (Fig. 6). By evaluating the validity of each beam on a per cycle basis, we are able to retain a higher proportion of beams and thus achieve better reconstruction accuracy, albeit from a constantly varying subset of beams.

Fig. 7, generated using the same 15-beam subset as Fig. 4, highlights the importance of temporal resolution in this application. The

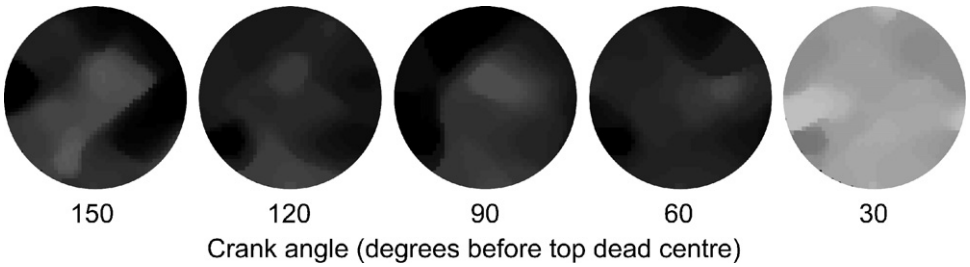

Fig. 6. The benefits of fully dynamic data selection. Images corresponding to the first row of Fig. 4 generated using the 21-beam subset resulting from data selection on a cycle-by-cycle basis. The images are significantly closer to the expected homogeneous result than those in Fig. 4, as would be expected from the relative performance of the two subsets during reconstruction of simulated data.

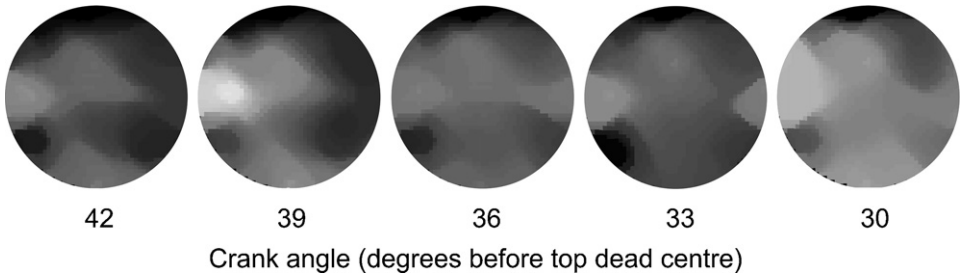

Fig. 7. Five images showing rapid changes in the period from 42° to 30° before TDC at intervals of 3° of crank angle (1500 rpm/1.5 bar BMEP load) obtained using the same 15-beam subset as Fig. 4.

five images span the range of crank angle from 42 °CA to 30 °CA before TDC, in 3 °CA (0.33 ms) increments (the final frame coincides with that shown at the top right of Fig. 4). Even on this relatively fine scale, very significant changes take place between frames. A progressive and rapid increase in HC concentration is evident, particularly as TDC is approached. It should be stressed that the relatively smooth frame-to-frame progression seen here is not the result of applied temporal filtering; each frame is the product of temporally independent measurement data and reconstruction.

4. Conclusion

We have described the first application of CST to the imaging of HC distributions within a multi-cylinder engine. Despite the low spatial resolution that inevitably results from the limited number of beam paths that can be accommodated, it has proved possible to obtain images that exhibit spatial and temporal characteristics in line with the expected behaviour of the engine, under the selected running conditions. At present, only relative distributions are claimed, due to the lack of sufficient opportunities for quantitative validation within the engine, but the use of a pressure-dependent absorption coefficient does, in principle, allow direct comparison of frames across crank angle.

The temporal resolution is extremely good, offering access to sub-cycle phenomena within the combustion chamber, with imaging rates well above the present 120 frames per engine revolution being possible if required. The system's continuous imaging capability is highly relevant in the investigation of non-repetitive events, such as cold starting and pre-ignition. Although recent advances in PLIF [21] have provided a continuous imaging capability, its extensive optical access requirement is still a severe limitation in respect of standard, multi-cylinder engines. We therefore continue to consider the two techniques as highly complementary. Improvements made in this second generation system, relative to that reported in [4], have enhanced the validity of the dual-wavelength ratiometric approach and have allowed adequate SNR to be maintained, despite increases in both bandwidth and source modulation frequency. The system is therefore well placed to address emerging trends in engine design, particularly gasoline direct injection (GDI). It is anticipated that recent advances in fibre laser and amplifier technology will increase the available optical power in the near future, bringing about further SNR improvement.

The OPAL concept has been largely successful in respect of sealing, thermal performance, mechanical integrity and operability both within and outside of the engine; we recommend the approach to others seeking multipoint access to the combustion chamber or similar environments. The 'minimally invasive' nature of the optical access is an important feature of our technique as it helps to ensure that the measurement itself does not change the behaviour of the engine. Larger scale optical access inevitably affects the thermal characteristics of the engine, and is extremely difficult to achieve in a multi-cylinder engine. CST has unique potential to be applied at several stages within an engine's development, starting with flow bench studies and culminating in performance validation of the final engine. It is hoped that this will enhance links between research studies, e.g. those carried out in single-cylinder 'glass-walled' engines, and practical vehicle implementations using multi-cylinder engines.

The production of the OPAL was a significant optical and mechanical engineering challenge. Perhaps inevitably for the first iteration of such a complex construction, the result is imperfect; some beam paths suffered from slight alignment shifts during manufacture, resulting in increased insertion loss. Overall, though, its performance has been adequate, allowing the use of between 23 and 26 beam paths during laboratory tests on propane plumes [19] and, even after a substantial period of fired operation in the engine, 15 beams retained sufficient SNR over several consecutive cycles to be used within this validation study. An even higher proportion of beams is available if dynamic data selection is performed on a cycle by cycle basis. No outright beam failures occurred over a substantial period of fired running (>2 h), despite operation over a wider range of loads and speeds than would have been possible in a 'glass-walled' engine.

Considerable effort was necessary to establish both the pre-processing of the beam path data and the subsequent reconstruction procedure for the present application. Uncontrolled factors will always be present so the development of effective methods for dealing with their influence on the measurement data was essential. Various approaches to referencing were evaluated, leading us to select comparison of fired versus motored cycles, in preference to intra-cycle referencing. Optimisation of the image reconstruction parameters has also been carried out; the laboratory test data were found to converge readily [19] but data obtained from the combustion chamber still require considerable user skill in both data selection and reconstruction if reliable images are to be obtained.

Unsurprisingly, for such an underdetermined problem, the accuracy of the image reconstruction is limited. Comparison with results obtained from simulated measurement data has proved useful in understanding the limitations of the reconstruction process, particularly in respect of image artefacts. Departure from the expected homogeneous validation condition has been found to be very similar to that obtainable using noise-free simulated data. Similar image artefacts are present in the measured and simulated cases, with evident dependence upon the beam subset selected. The various trials that preceded the collection of the validation data considered here were essential in the development of the skip-motoring and referencing strategies. However, in future studies, the lack of such preliminary activities will allow data collection earlier in the service life of the OPAL, providing higher SNR on the majority of beams and more serviceable beams overall, allowing the full performance potential of a new OPAL to be realised.

In conclusion, viable solutions have been developed in the key areas of optical access to the combustion chamber, high-speed DWR transmission measurement, and the reconstruction of the resulting irregular and sparse datasets, together enabling a demonstration of CST within a minimally modified multi-cylinder engine. The calculated spatial distributions are consistent with expectation, within limits imposed by the extremely underdetermined nature of the measurement, and the inherently high temporal resolution offers an arguably unique insight into the behaviour of the HC fuel within a multi-cylinder engine.

Acknowledgements

The authors acknowledge the support received for the IMAGER project from the then UK Department of Trade and Industry (DTI) and the Engineering and Physical Sciences Research Council (EPSRC). Particular thanks go to Steve Gratze at DTI for his contributions, both strategic and technical.

References

[1] R. Stone, Introduction to Internal Combustion Engines, 3rd ed., Macmillan Press, London, 1999.
[2] V. Sick, H. McCann, in: D. Scott, H. McCann (Eds.), Process Imaging For Automatic Control, CRC Press, Boca Raton, 2005.
[3] S.J. Carey, H. McCann, F.P. Hindle, K.B. Ozanyan, D.E. Winterbone, E. Clough, Chemical species tomography by near infra-red absorption, Chem. Eng. J. 77 (1–2) (2000) 111–118.
[4] F.P. Hindle, S.J. Carey, K.B. Ozanyan, D.E. Winterbone, E. Clough, H. McCann, Measurement of gaseous hydrocarbon distribution by a near-infra-red absorption tomography system, J. Electron. Imag. 10 (3) (2001) 593–600.
[5] H. Zhao, N. Ladommatos, Optical Diagnostics for In-cylinder mixture formation measurements in IC engines, Prog. Energy Combust. Sci. 24 (4) (1998) 297–336.
[6] M. Richter, Z.S. Li, M. Alden, Application of two-photon laser-induced fluorescence for single-shot visualization of carbon monoxide in a spark ignited engine, Appl. Spectrosc. 61 (1) (2007) 1–5.
[7] C. Schulz, V. Sick, Tracer-LIF diagnostics: quantitative measurement of fuel concentration, temperature and fuel/air ratio in practical combustion systems, Prog. Energy Combust. Sci. 31 (1) (2005) 75–121.
[8] Philipp H., Plimon A., Fernitz G., Hirsch A., Fraidl G., Winklhofer E., A tomographic camera system for combustion diagnostics in SI engines, *SAE950681*, 1995.
[9] R. Snyder, L. Hesselink, Measurement of mixing fluid flows with optical tomography, Opt. Lett. 13 (2) (1988) 87–89.
[10] R.J. Santoro, H.G. Semerjian, P.J. Emmerman, R. Goulard, Optical tomography for flow field diagnostics, Int. J. Heat Mass Trans. 24 (7) (1981) 1139–1150.
[11] E.J. Beiting, Fiberoptic fan-beam absorption tomography, Appl. Opt. 31 (9) (1992) 1328–1343.
[12] E.D. Torniainen, F.C. Gouldin, Tomographic reconstruction of 2-D absorption coefficient distributions from a limited set of infrared absorption data, Combust. Sci. Technol. 131 (1–6) (1998) 85–105.
[13] A. Barrag, B. Lawton, Computer optical tomography in the study of internal combustion engine soot concentration, in: Proceedings of 26th International Symposium Automotive Technology and Automation, Vol. The Motor Vehicle and the Environment — Demands of the Nineties and Beyond (ISATA, 1993), 1993, pp. 423–480.
[14] S. Shimizu, S. Sakai, High-speed tomography for simultaneous measurement of the histories of two-dimensional distributions of temperature and density of burnt gases, JSME Int. J. Ser. B – Fluids Therm. Eng. 37 (3) (1994) 596–603.
[15] H. Krämer, S. Einecke, C. Schulz, V. Sick, S.R. Nattras, J.S. Kitching, Simultaneous mapping of the distribution of different fuel volatility classes using tracer LIF and NIR tomography in an IC engine, SAE Trans., J. Fuels Lubric. 107 (1998) 1048–1059.
[16] J.A. Drallmeier, Hydrocarbon-vapor measurements in pulsed fuel sprays, Appl. Opt. 33 (33) (1994) 7781–7788.
[17] P. Wright, C.A. Garcia-Stewart, S.J. Carey, F.P. Hindle, S. Pegrum, S. Colbourne, P. Turner, W. Hurr, T. Litt, S.C. Murray, S.D. Crossley, K.B. Ozanyan, H. McCann, Toward in-cylinder absorption tomography in a production engine, Appl. Opt. 44 (31) (2005) 6578–6592.
[18] K. Salem, E. Tsotsas, D. Mewes, Tomographic measurements of breakthrough in a packed bed adsorber, Chem. Eng. Sci. 60 (2) (2005) 517–522.
[19] N. Terzija, J.L. Davidson, C.A. Garcia-Stewart, P. Wright, K.B. Ozanyan, S. Pegrum, T.J. Litt, H. McCann, Image optimisation for chemical species tomography with an irregular and sparse beam array, Meas. Sci. Technol. 19 (2008) 094007.
[20] P. Wright, K.B. Ozanyan, S.J. Carey, H. McCann, Design of high-performance photodiode receivers for optical tomography, IEEE Sens. J. 5 (2) (2005) 281–288.
[21] J.D. Smith, V. Sick, Quantitative, dynamic fuel distribution measurements in combustion-related devices using laser-induced fluorescence imaging of biacetyl in iso-octane, Proc. Comb. Inst. 31 (2007) 747–755.